Generating Non-Rayleigh Speckles with Tailored Intensity Statistics

Yaron Bromberg,* and Hui Cao,†
Department of Applied Physics, Yale University, New Haven, Connecticut 06520, USA
(Received 29 January 2014; published 29 May 2014)

We experimentally generate speckle patterns with non-Rayleigh statistics using a phase-only spatial light modulator. By introducing high order correlations to the input light fields we redistribute the intensity among the speckle grains, while preserving the granular structure of the pattern. Our method is versatile and allows for generating speckle patterns with enhanced or diminished contrast in a controlled manner.

DOI: 10.1103/PhysRevLett.112.213904 PACS numbers: 42.25.Dd, 42.25.Fx, 42.30.Ms

Speckle patterns appear whenever a coherent wave impinges upon a scattering sample. The granular structure of speckles results from the sensitivity of the interference pattern to the relative phases of the scattered partial waves. As speckle formation is essentially a wave phenomena, it has been observed for a wide range of waves of different nature, including ultrasonic waves [1], microwaves [2,3], optical waves [4], x rays [5], and matter waves [6]. In spite of the diverse settings in which speckles appear, they usually show universal statistical properties, known as Rayleigh statistics. The amplitudes of the speckle field are distributed according to the Rayleigh distribution, resulting in a negative exponential intensity distribution [4]. An interesting question is whether the spatial structure of speckle patterns necessarily dictates Rayleigh statistics, or perhaps it is possible to tailor the distribution of the intensities among the speckle grains while maintaining the random granular pattern.

The reason that speckle patterns typically exhibit Rayleigh statistics is that Rayleigh statistics emerge under rather general conditions: the field is a sum of a large number of partial waves with independently varying amplitudes and phases, and the phases are uniformly distributed over a range of 2π. In the weak scattering regime the latter condition is not satisfied; hence, non-Rayleigh speckles with a low contrast and a strong dc background are formed [7]. Similarly, in the near-field zone of a scattering media where just a small number of scattered partial waves is detected and the relative phase of these waves does not cover the full 2π range, low contrast speckles with nonuniversal statistics are observed [8–10]. In the strong scattering regime where the phases are uniformly distributed, deviations from Rayleigh statistics can be observed for a small number of partial waves, but the statistics approaches Rayleigh statistics as the number of partial waves is increased [11]. For generating speckles with robust non-Rayleigh statistics that result from redistribution of the intensity among the speckle grains, we need to consider the interference of a large number of partial waves whose phases are uniformly distributed over a range of 2π. In this case the only way to observe non-Rayleigh speckles is to make the complex amplitudes of the partial waves statistically dependent. Multiple scattering can introduce mesoscopic correlations that modify Rayleigh statistics due to strong fluctuations in the total power that is transmitted through the sample [12]. However, for a single random configuration, the distribution of the intensity between the speckle grains is a negative exponential, indicating that the speckle field still follows Rayleigh statistics [13,14]. Similarly, non-Rayleigh statistics are observed when the total power that is incident on a scattering sample fluctuates [4] or when two identical speckle patterns with a fluctuating relative phase are interfered [15], yet, per realization, each speckle pattern exhibits Rayleigh statistics. We, on the other hand, are seeking to redistribute the light among the speckle grains, so that individual speckle patterns will also exhibit non-Rayleigh statistics.

In this Letter we show how to tailor the speckle statistics using a phase-only spatial light modulator (SLM) that is illuminated by a laser beam. The SLM pixels mimic scattering from a rough surface, and the diffraction from each pixel corresponds to a partial wave that is scattered from the SLM plane. We record the speckle patterns at the Fourier plane of the SLM; where the intensity statistics are determined by the statistical properties of the phase matrices that are applied to the SLM. We developed a simple method for finding the phase matrices that yield non-Rayleigh speckles, i.e., speckle patterns with an intensity distribution that deviates from a negative exponential. Since speckle patterns are a valuable resource for both fundamental research [2,13,14,16–20] and numerous applications [21–29], a control of the intensity statistics can have a dramatic impact on the way we use and analyze speckles. For example, one can utilize tailored speckles to synthesize the statistics of disordered optical potentials for cold atoms and colloidal particles [30–32], or optimize the intensity statistics per application in speckle illumination imaging [26–29]. Since speckle patterns are intimately related to the statistical properties of thermal light sources, temporally fluctuating patterns are often used as pseudo-thermal light sources. Using fluctuating non-Rayleigh

speckles it would be possible to generate pseudothermal sources which violate the Siegert relation and exhibit a bunching factor $g^{(2)}(0) \neq 2$, with potential applications such as studying classical models of extrabunching [33,34] and high-order ghost imaging [35].

To experimentally demonstrate our method for generating non-Rayleigh speckles, we start with an example for enhancing the contrast of a speckle pattern. We use a phase-only reflective SLM, which is illuminated by a linearly polarized laser beam with diameter $D = 5$ mm. The SLM pixels are grouped to macropixels providing a control over 3000 independent phase elements. We place the SLM at the front focal plane of a lens and record the intensity pattern at the Fourier plane of the SLM by imaging the back focal plane of the lens (see [36] for additional details). When we apply to the SLM a random uncorrelated phase matrix, a Rayleigh speckle pattern is observed at the Fourier plane [Fig. 1(a)]. To generate a speckle pattern with an enhanced contrast, we must send to the SLM a phase matrix with correlated pixels. To find such a matrix, we first numerically generate a high contrast speckle, for example, by squaring the field of a standard Rayleigh speckle, $E^2_{\mathrm{Ray}}(x, y)$. Next, we compute the inverse Fourier transform, and apply the phase of the inverse Fourier transform to the SLM. Figure 1(b) shows the resulting speckle pattern of a phase matrix computed in this way. It is clearly seen that the distribution of the intensities among the speckle grains is different than for Rayleigh speckles [Fig. 1(a)]; a few grains are much brighter than the rest. Indeed, the intensity histogram collected from all the points in the Fourier plane and over a 1000 speckle realizations decays slower than a negative exponential, featuring the high probability to obtain bright speckle grains [Fig. 1(d), green diamonds]. We note that the histogram collected from a single point in the Fourier plane follows the exact same statistics [36]. The contrast of the patterns, defined as $C = \sqrt{\langle I^2 \rangle / \langle I \rangle^2 - 1}$, where $\langle \cdots \rangle$ denotes spatial averaging over the entire Fourier plane, and an ensemble averaging, is $C = 1.28$. It is significantly higher than the contrast measured for the Rayleigh speckles $C = 0.98$. We coin this kind of high contrast patterns super-Rayleigh speckles.

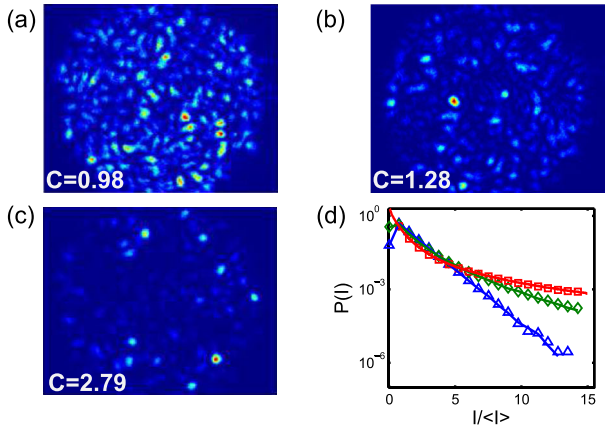

FIG. 1 (color online). Experimental generation of super-Rayleigh speckles. (a)–(c) Images of the speckle patterns at the Fourier plane of the SLM, and (d) the corresponding intensity distribution function. (a) Standard Rayleigh speckles with a contrast of $C = 0.98$ and a negative exponential intensity distribution [(d), blue triangles]. (b) Super-Rayleigh speckles with a contrast of $C = 1.28$, and an intensity distribution that decays slower than the negative exponential [(d), green diamonds]. The light is concentrated at a fewer speckle grains compared to (a), resulting in an enhanced probability to detect high intensities. (c) Higher contrast super-Rayleigh speckles with $C = 2.79$ and a long tailed intensity histogram [(d), red squares]. Solid lines are histograms obtained for the normalized speckle patterns (see text).

Instead of squaring the Rayleigh speckle field E_{Ray} as in the example above, in principle, we can use any nonlinear transformation $h(E_{\mathrm{Ray}})$ to obtain non-Rayleigh speckle. Thus, we can generate super-Rayleigh speckles with a higher contrast by using, for example, the fourth power of the speckle field $h(E_{\mathrm{Ray}}) = E^4_{\mathrm{Ray}}$. We send to the SLM the phase of the inverse Fourier transform of E^4_{Ray}, and observe patterns with $C = 2.79$ [Fig. 1(c)] and a long tailed intensity histogram [Fig. 1(d), red squares]. We note that the long tailed intensity histograms of super-Rayleigh speckles result from redistribution of the intensity among the speckle grains and not because of fluctuations in the total intensity of different speckle realizations. To verify this, we normalize all the speckle patterns to have the same total intensity, and show that the intensity histograms of the normalized and non-normalized patterns are identical [Fig. 1(d), solid lines].

The super-Rayleigh speckle statistics arises from concentrating the light to a fewer bright grains compared to Rayleigh speckles. It is interesting to explore the opposite regime which we coin sub-Rayleigh speckles, where the light is distributed in a more homogenous manner among the grains. Intuitively, saturation of the intensity can reduce the intensity fluctuations and the speckle contrast, while preserving the granular structure of the speckles. Thus, we use a nonlinear transformation that saturates the amplitude of a Rayleigh speckle, but keeps its phase untouched, $h(E_{\mathrm{Ray}}) = \sqrt{1 - e^{-|E_{\mathrm{Ray}}|^2}} e^{i\theta_{\mathrm{Ray}}}$, where $\theta_{\mathrm{Ray}} = \arg(E_{\mathrm{Ray}})$ is the phase of the Rayleigh speckle field. Unlike super-Rayleigh speckles, where we applied to the SLM the phase of the inverse Fourier transform of $h(E_{\mathrm{Ray}})$ and observed a pattern that to a good approximation matched $h(E_{\mathrm{Ray}})$, for sub-Rayleigh speckles when we keep only the phase of the inverse Fourier transform of $h(E_{\mathrm{Ray}})$ and disregard the amplitude variation, we observe nearly standard Rayleigh speckles. This is because the amplitude modulation encodes much information of the transformed speckle. To transfer this information to phase modulation, we apply an iterative procedure based on the Gershberg-Saxton algorithm [37], where using Fourier transforms we numerically

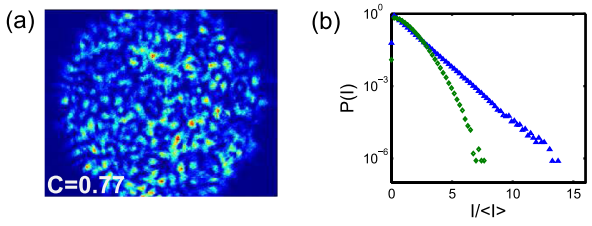

FIG. 2 (color online). (a) A speckle pattern measured at the Fourier plane of the SLM, using a phase matrix that was designed to generate sub-Rayleigh speckles. The low contrast of the pattern results from a more homogenous distribution of the intensity among the speckle grains compared to Rayleigh speckles. (b) Measured intensity distribution function of the sub-Rayleigh speckles (green diamonds), which decays much faster than the negative exponential observed for Rayleigh speckles (blue triangles).

propagate the field back and forth between the SLM plane and the Fourier plane. At each iteration step we fix the amplitude at the Fourier plane to be $\sqrt{1-e^{-|E_{\mathrm{Ray}}|^2}}$, and we set the amplitude at the SLM plane to match the amplitude of the beam profile that impinges on the SLM. After 50 iterations the algorithm converges to a speckle pattern at the Fourier plane with an intensity pattern that is proportional to $1-e^{-|E_{\mathrm{Ray}}|^2}$ and a corresponding phase matrix at the SLM plane. We repeat the algorithm with different initial Rayleigh speckles E_{Ray} to generate a set of a phase matrices, which we then send to the SLM. The recorded patterns indeed show a low contrast ($C = 0.77$), and the intensity histogram decays faster than a negative exponential (Fig. 2). By comparing Fig. 2(a) to Fig. 1(a), it can be seen that intensity distribution among the speckle grains of the sub-Rayleigh speckles is more homogenous, which is the origin of the lower contrast.

One interesting feature of the non-Rayleigh speckles is that the speckle statistics change as the beam propagates. All the results presented so far were measured at the Fourier plane of the SLM; however, when we scan the image plane away from the Fourier plane, the speckles gradually return to Rayleigh statistics [36]. Figure 3 shows the contrast of the recorded speckle patterns as a function of the distance between the Fourier plane and the plane that is imaged by the camera, showing that the contrast of the super-Rayleigh and sub-Rayleigh speckles is axially dependent, whereas the contrast of the Rayleigh speckle remains constant. The range over which the non-Rayleigh statistics are observed corresponds to the longitudinal length of a single speckle. This longitudinal length is equal to the Rayleigh range of an input Gaussian beam that is focused to a spot of the size of a single speckle [38]. It is therefore determined by the envelope of the beam that illuminates the SLM, and it is not modified by phase-only modulation.

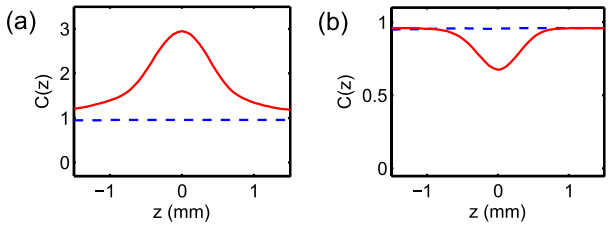

FIG. 3 (color online). Axially dependent speckle contrast. (a) The measured contrast of the speckle patterns versus the distance from the Fourier plane, for Rayleigh (blue dashed line) and super-Rayleigh (red line) speckles. (b) Same as (a) for sub-Rayleigh speckles. The width of the contrast peak or dip corresponds to the longitudinal length of a single speckle.

Observing non-Rayleigh statistics necessarily implies that the fields at the SLM plane break at least one of the two conditions for observing Rayleigh speckles: either the phases are not uniformly distributed over 2π, or the fields at different pixels are correlated. Figure 4(a) shows the histograms of the phases that were used to generate Rayleigh speckles (blue triangles), super-Rayleigh speckles (green diamonds), and sub-Rayleigh speckles (red squares). All three histograms are constant over $[0, 2\pi]$, which means that the non-Rayleigh statistics must originate from correlations between the SLM pixels. We therefore look at the correlation of the field at the SLM plane $G^{(1)}_{\mathrm{SLM}}(\Delta_x, \Delta_y) = \langle E_{\mathrm{SLM}}(x, y) E^{*}_{\mathrm{SLM}}(x+\Delta_x, y+\Delta_y)\rangle$. We obtain $G^{(1)}_{\mathrm{SLM}}$ using the generalized van Cittert–Zernike theorem [4] by computing the Fourier transform of the average intensity pattern at the Fourier plane of the SLM. The $G^{(1)}_{\mathrm{SLM}}$ curves for super- and sub-Rayleigh speckles are presented in Fig. 4(b), showing that fields at different macropixels are uncorrelated. The question is then how can uncorrelated fields with phases that are uniformly distributed over 2π yield non-Rayleigh statistics? The answer is

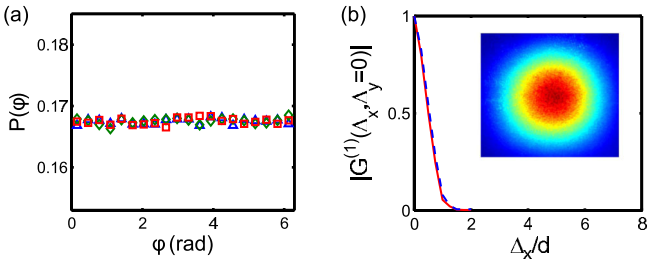

FIG. 4 (color online). (a) Histograms of the phases used to generate Rayleigh (blue triangles), super-Rayleigh (green diamonds), and sub-Rayleigh (red squares) speckles. All three histograms are constant over 2π. (b) The field correlation at the SLM plane $G^{(1)}_{\mathrm{SLM}}$ for super-Rayleigh speckle (blue dashed line) and sub-Rayleigh speckle (red solid line). $d = 80\ \mu$m is the size of 1 macropixel. Fields separated by more than 1 macropixel are uncorrelated, indicating that the source of the non-Rayleigh statistics is in higher order correlations. The inset shows the average intensity for the sub-Rayleigh speckles, from which $G^{(1)}_{\mathrm{SLM}}$ was computed.

TABLE I. Numerical evaluation of $\Gamma_p^{(2)}$, the second order correlation between fields at p different pixels, for speckles of different statistics. The cross correlation between fields at four different pixels $\Gamma_4^{(2)}$ is the source of the non-Rayleigh statistics.

	$\Gamma_1^{(2)}$	$\Gamma_2^{(2)}$	$\Gamma_3^{(2)}$	$\Gamma_4^{(2)}$
Rayleigh	0.0	2.0	0.0	**0.0**
Super-Rayleigh $h(E) = E^2$	0.0	2.0	0.0	**0.7**
Super-Rayleigh $h(E) = E^4$	0.0	2.0	0.0	**5.6**
Sub-Rayleigh	0.0	2.0	0.0	**−0.4**

that $G^{(1)}_{\mathrm{SLM}}(\Delta) = 0$ indicates that fields separated by a distance Δ are uncorrelated, but it does not necessarily mean that the fields are statistically independent. For non-Gaussian random fields, higher order correlations can exist even if the first order correlation vanishes [39].

To investigate the role of higher order correlations in the formation of non-Rayleigh speckles, we study numerically the contribution of the second-order field correlations to the contrast of the speckle patterns. Since the laser beam is linearly polarized and the scattering angles from the SLM are too small to introduce radial polarization, we consider scalar fields. A partial wave that diffracts from an SLM pixel at position $\mathbf{r}$ to position $\boldsymbol{\rho}$ in the Fourier plane is proportional to $e^{i(\psi_{\mathbf{r}} - 2\pi\boldsymbol{\rho}\mathbf{r}/\lambda f)}$, where $\psi_{\mathbf{r}}$ represents the SLM phase at $\mathbf{r}$, λ is the optical wavelength and f is the focal length of the lens that performs the Fourier transform. The square of the contrast of the speckle pattern at the Fourier plane is, therefore,

$$C^2 \equiv \langle I^2\rangle - \langle I\rangle^2 = \left\langle \int d^2\boldsymbol{\rho}|E(\boldsymbol{\rho})|^4 \right\rangle_e - 1 = \frac{1}{N^2}\sum_{\mathbf{r_1},\mathbf{r_2},\mathbf{r_3}\mathbf{r_4}} \langle \mathbf{e}^{\mathbf{i}(\psi_{\mathbf{r}_1}+\psi_{\mathbf{r}_2}-\psi_{\mathbf{r}_3}-\psi_{\mathbf{r}_4})}\rangle_{\mathbf{e}} \delta_{\mathbf{r}_1+\mathbf{r}_2-\mathbf{r}_3,\mathbf{r}_4} - 1, \quad (1)$$

where N is the number of SLM pixels, $\langle\cdots\rangle_e$ denotes ensemble averaging, and $\langle I\rangle$ is normalized to 1. The sum on the right-hand side is in fact a sum over the second order correlation between the fields at all the SLM pixels: $\sum G^{(2)}_{\mathrm{SLM}}(\mathbf{r_1},\mathbf{r_2},\mathbf{r_3},\mathbf{r_1}+\mathbf{r_2}-\mathbf{r_3})$. We can decompose this sum into 4 terms, $C^2 = \Gamma_1^{(2)} + \Gamma_2^{(2)} + \Gamma_3^{(2)} + \Gamma_4^{(2)} - 1$, where $\Gamma_p^{(2)}$ is the second order correlation between fields at p different pixels, e.g., $\Gamma_4^{(2)} = \sum_{\mathbf{r_1}\neq\mathbf{r_2}\neq\mathbf{r_3}\neq\mathbf{r_4}} \times G^{(2)}_{\mathrm{SLM}}(\mathbf{r_1},\mathbf{r_2},\mathbf{r_3},\mathbf{r_1}+\mathbf{r_2}-\mathbf{r_3})$. For Rayleigh speckles that are formed by statistically independent pixels, only correlations of fields at the same pixel contribute to the sum, hence, $\Gamma_1^{(2)} = 1/N$, $\Gamma_2^{(2)} = 2 - 2/N$ and $\Gamma_3^{(2)} = \Gamma_4^{(2)} = 0$. For non-Rayleigh speckles, we evaluate $\Gamma_p^{(2)}$ numerically by calculating the second order correlations $G^{(2)}_{\mathrm{SLM}}(\mathbf{r_1},\mathbf{r_2},\mathbf{r_3},\mathbf{r_4} = \mathbf{r_1}+\mathbf{r_2}-\mathbf{r_3})$ for all the combinations of the indices $\{\mathbf{r_1},\mathbf{r_2},\mathbf{r_3},\mathbf{r_4}\}$, and decomposing the results into the four terms $\Gamma_p^{(2)}$ according to the number of different indices that appear in each combination. The numerical results for 5000 phase patterns with 100 pixels are summarized in Table 1. It is seen that the source of the non-Rayleigh statistics is $\Gamma_4^{(2)}$, i.e., the cross correlation between four *different* pixels.

In Eq. (1) the high order correlations of the field at the SLM plane are linked to the intensity statistics at the Fourier plane. However, for points that are not in the Fourier plane an additional quadratic phase factor $e^{i\pi z(\mathbf{r_1}^2+\mathbf{r_2}^2-\mathbf{r_3}^2-\mathbf{r_4}^2)/\lambda f^2}$ multiplies each term in the right-hand side of Eq. (1), where z is axial to the distance from the Fourier plane. Because of this quadratic phase the high order correlations do not add in phase and their contribution to the intensity statistics vanishes. This is the reason why we observe non-Rayleigh statistics only at the Fourier plane of the SLM. We note that by adding a quadratic phase to the SLM it is possible to shift the axial position of the Fourier plane where the speckle statistics is non Rayleigh.

In conclusion, we developed a method to generate speckle patterns with controlled intensity statistics. In contrast to previous works that used an SLM to control the spatial coherence of light fields by shaping the spatial frequency distribution [40–42] or synthesizing the coherent mode decomposition of the field [43], we use the SLM to redistribute the intensity among the speckle grains. We link the observed non-Rayleigh statistics to higher order correlations of the scattered partial waves, paving the way towards a better understanding of the information carried by speckles that are scattered from disordered samples with structural correlations. Non-Rayleigh speckles also offer new opportunities for speckle illumination applications. On one hand, the axially varying contrast of super-Rayleigh speckles can be utilized for achieving better optical sectioning in speckle illumination microscopy. On the other hand, the homogenous distribution of sub-Rayleigh speckles are attractive for imaging modalities that utilize speckle illumination, as it can reduce the number of projections required for averaging the speckles to observe a smooth image and enhance the image acquisition rate. Therefore, tailored speckles allow optimizing the intensity statistics for target applications.

We thank Eric Dufresne, Brandon Redding, Sebastien Popoff and Arthur Goetschy for fruitful discussions. This work is supported partially by NSF under the Grants No. ECCS1128542 and No. DMR1205307.

*yaron.bromberg@yale.edu
†hui.cao@yale.edu

[1] R. Wagner, S. Smith, J. Sandrik, and H. Lopez, IEEE Trans. Sonics Ultrason. **30**, 156 (1983).
[2] J. Wang and A. Z. Genack, Nature (London) **471**, 345 (2011).

[3] J. S. Lee, Computer Graphics and Image Processing **17**, 24 (1981).
[4] J. W. Goodman, *Speckle Phenomena in Optics: Theory and Applications* (Roberts and Co., Englewood, 2007).
[5] M. Sutton, S. G. J. Mochrie, T. Greytak, S. E. Nagler, L. E. Berman, G. A. Held, and G. B. Stephenson, Nature (London) **352**, 608 (1991).
[6] R. G. Dall, S. S. Hodgman, A. G. Manning, M. T. Johnsson, K. G. H. Baldwin, A. G. Truscott, Nat. Commun. **2**, 291 (2011).
[7] W. T. Welford, Contemp. Phys. **21**, 401 (1980).
[8] J.-J. Greffet and R. Carminati, Ultramicroscopy **61**, 43 (1995).
[9] A. Apostol and A. Dogariu, Phys. Rev. Lett. **91**, 093901 (2003).
[10] A. Apostol and A. Dogariu, Phys. Rev. E **72**, 05602(R) (2005).
[11] J. W. Goodman, Appl. Opt. **47**, A111 (2008).
[12] T. M. Nieuwenhuizen and M. C. W. van Rossum, Phys. Rev. Lett. **74**, 2674 (1995).
[13] A. Z. Genack and A. A. Chabanov, J. Phys. A **38**, 10 465 (2005).
[14] T. Strudley, T. Zehender, C. Blejean, E. P. A. M. Bakkers and O. L. Muskens, Nat. Photonics **7**, 413 (2013).
[15] P. Hong, J. Liu, and G. Zhang, Phys. Rev. A **86**, 013807 (2012).
[16] D. J. Pine, D. A. Weitz, P. M. Chaikin and E. Herbolzheimer, Phys. Rev. Lett. **60**, 1134 (1988).
[17] F. Scheffold and G. Maret, Phys. Rev. Lett. **81**, 5800 (1998).
[18] W. Langbein, J. M. Hvam, and R. Zimmermann, Phys. Rev. Lett. **82**, 1040 (1999).
[19] F. Ferri, D. Magatti, A. Gatti, M. Bache, E. Brambilla, and L. A. Lugiato, Phys. Rev. Lett. **94**, 183602 (2005).
[20] T. Schwartz, G. Bartal, S. Fishman, and M. Segev, Nature (London) **446**, 52 (2007).
[21] A. C. Völker, P. Zakharov, B. Weber, F. Buck, and F. Scheffold, Opt. Express **13**, 9782 (2005).
[22] D. A. Boas and A. K. Dunn, J. Biomed. Opt. **15**, 011109 (2010).
[23] N. Curry, P. Bondareff, M. Leclercq, N. F. van Hulst, R. Sapienza, S. Gigan, and S. Grésillon, Opt. Lett. **36**, 3332 (2011).
[24] F. Scheffold and I. D. Block, Opt. Express **20**, 192 (2012).
[25] B. Redding, S. F. Liew, R. Sarma, and H. Cao, Nat. Photonics **7**, 746 (2013).
[26] M. C. Pitter, C. W. See, and M. G. Somekh, Opt. Lett. **29**, 1200 (2004).
[27] D. Lim, K. K. Chu, and J. Mertz, Opt. Lett. **33**, 1819 (2008).
[28] E. Mudry, K. Belkebir, J. Girard, J. Savatier, E. Le Moal, C. Nicoletti, M. Allain, and A. Sentenac, Nat. Photonics **6**, 312 (2012).
[29] J. Gateau, T. Chaigne, O. Katz, S. Gigan, and E. Bossy, Opt. Lett. **38**, 5188 (2013).
[30] J. Billy, V. Josse, Z. Zuo, A. Bernard, B. Hambrecht, P. Lugan, D. Clément, L. Sanchez-Palencia, P. Bouyer, and A. Aspect, Nature (London) **453**, 891 (2008).
[31] K. M. Douglass, S. Sukhov, and A. Dogariu, Nat. Photonics **6**, 834 (2012).
[32] G. Volpe, G. Volpe, and S. Gigan, Sci. Rep. **4**, 3936 (2014).
[33] F. Boitier, A. Godard, N. Dubreuil, P. Delaye, C. Fabre, and E. Rosencher, Nat. Commun. **2**, 425 (2011).
[34] T. S. Iskhakov, A. Perez, K. Y. Spasibko, M. V. Chekhova, and G. Leuchs, Opt. Lett. **37**, 1919 (2012).
[35] K. W. C. Chan, M. N. O'Sullivan, and R. W. Boyd, Opt. Express **18**, 5562 (2010).
[36] See Supplemental Material at http://link.aps.org/supplemental/10.1103/PhysRevLett.112.213904 for a detailed description of the setup, an analysis of local deviations from Rayleigh statistics, and measurements of the three dimensional structure of the speckle patterns.
[37] R. W. Gerchberg and W. O. Saxton, Optik **35**, 227 (1972).
[38] A. Gatti, D. Magatti, and F. Ferri, Phys. Rev. A **78**, 063806 (2008).
[39] L. Mandel and E. Wolf, *Optical Coherence and Quantum Optics* (Cambridge University Press, Cambridge, England, 1995).
[40] H. Funamizu and J. Uozumi, Opt. Express **15**, 7415 (2007).
[41] L. Waller, B. Situ and J. W. Fleischer, Nat. Photonics **6**, 474 (2012).
[42] C. Sun, L. Waller, D. V. Dylov, and J. W. Fleischer, Phys. Rev. Lett. **108**, 263902 (2012).
[43] B. Rodenburg, M. Mirhosseini, O. S. Magaña-Loaiza, and R. W. Boyd, J. Opt. Soc. Am. B **31**, A51 (2014).